Journal of Applied Electrochemistry (2006) 36:363–368
DOI 10.1007/s10800-005-9078-7

In situ electrochemical scan to study the behavior of the asymmetric (single-side) pasted positive plate as used in automotive lead-acid batteries

YONGLANG GUO
College of Chemistry and Chemical Engineering, Fuzhou University, Fuzhou, 350002, P.R.China
(E-mail: yguo@fzu.edu.cn)

Received 16 December 2004; accepted in revised form 22 September 2005

Key words: current and potential distributions, lead-acid batteries, pasting, positive plate

Abstract

The performance of a asymmetric (single-side) pasted positive plate was studied by measuring the current density and potential distributions on both sides of the plate. It was found that the current densities on both sides are almost the same during the early discharge at the 3 C discharge rate. As the discharge proceeds, the current decreases gradually on the non-pasted side and increases on the pasted side. Since more active mass exists on the pasted side, the matrix resistance is higher, causing the polarization to increase by 55–90 mV at the 3 C discharge rate. On the non-pasted side, the active mass undergoes a deeper depth of discharge (DOD). This leads to the shedding of active mass, which shortens the battery life. Since the positive grid on the non-pasted side is exposed, its corrosion rate is faster.

1. Introduction

Although lead-acid batteries are widely used, the positive plate is still a focus of investigation. An important aspect of this is that the composition of the positive active mass (PAM) containing α-PbO_2, β-PbO_2 and PbO_n ($1 < n < 2$), etc. is complicated [1–4]. The PAM structure depends on its porosity and the ratio of α- to β-PbO_2, which determine the power output of the battery and its life [5]. The presence of small amounts of Sb in the grid alloy accelerates the corrosion of the positive grid. This is one of the important failure mechanisms occurring in lead-acid batteries with Pb-Sb alloy grids [6–9]. However, the Pb–Ca alloy (without Sb) in valve-regulated lead-acid (VRLA) batteries exhibits premature capacity loss (PCL-1). The addition of Sb is an effective way to overcome PCL-1 [10–14]. At present, the specific energy of lead-acid batteries is still relatively low due to low utilization of the active mass. Further, the relative utilization of PAM compared to that of the negative active mass (NAM) is lower. At low discharge rate, the PAM utilization is only about 50% for automotive lead-acid batteries and it becomes smaller with the increase of the discharge rate [15–17]. During the cycling of VRLA batteries, the swelling and shedding of the PAM leads to premature capacity loss (PCL-2) [18]. Besides compressing the plate stack, a usual way of prolonging the cycle life is to use more PAM, which makes the PAM utilization even lower [19]. The tubular positive plate design can solve the problem of swelling and shedding of PAM [20].

The performance of the positive plate is closely related to its processing methodology, particularly paste formulation, curing and formation [21–24]. The amount of H_2SO_4 and water used significantly affects the initial capacity of the battery and its life. Additives in the paste can be used to increase the PAM utilization and power output [25, 26]. The curing and formation play an important role in the cycle life of the lead-acid battery [27]. In the production of the positive plate, single-side pasting has been widely used. Although this pasted positive plate is asymmetrical, there is no report on the relative performance difference between the front and back of the single-side pasted positive plate. Therefore, it is of value to know the behavior of this kind of pasted plate and its consequent effects on the performance of the lead-acid batteries.

In our previous work [28, 29], an *in situ* electrochemical scan technique was established to measure the current and potential distributions on the lead-acid battery plates. In this paper this technique is used to further study the performances of the two sides of the asymmetric pasted positive plate used in automotive lead-acid batteries.

2. Experimental

The test plate was a commercial automotive positive plate made by Jin Fengfan Storage Battery Co. Ltd. It was produced by single-side pasting and had dimensions of 14.3 cm (W) × 13 cm (H) ×0.21 cm (T). The formed

positive plate is shown in Figure 1. Each positive plate contains about 138 g active mass. Its C_{20} capacity was 15 Ah.

To study the current and potential distributions on each side of the single-side pasted positive plate, an experimental set-up was described in detail in the previous work [28]. In short, the test positive plate was placed between two negative plates. The container used had the internal dimensions of 14.5 cm (W) $\times$ 9.0 cm (L) $\times$15 cm (H). The distance between the positive and negative plates was about 4.2 cm. When the positive plate was discharged, the IR voltage drop appeared in the electrolyte. To measure the local current density and potential, two $Hg/Hg_2SO_4/H_2SO_4$ (1.285 sp. gr.) reference electrodes were used to measure the local IR drop in the electrolyte and the local potential on the positive plate. The measurement distance of two reference electrode tips was 3 cm. 162 data points were obtained by scanning six pairs of reference electrodes from the bottom to top of the positive plate. The IR voltage drop and the electrode potentials were recorded by a HP 34970A Data Acquisition/Switch Unit connected to a PC. In the experiments, the positive plate was discharged at 45 A in the H_2SO_4 electrolyte of 1.285 specific gravity.

3. Results and discussion

To reduce the corrosion rate of the positive grid, the paste should wrap around the grid. However, by virtue of the pasting process used, the paste is pressed into the spaces between the ribs of the grid only from one side. There is a layer of paste about 0.2–0.5 mm thick on the front of the grid while the ribs of the grid on the back are not covered by paste. Figure 1 shows the photographs of both the pasted and non-pasted sides of the formed positive plate. Although the grid and the active mass have the same color, the radial current collector ribs are visible in Figure 1(a). Yet on the pasted side (Figure 1b), only PAM is observed because there is a 0.2 mm-thick layer of active mass over the grid.

In the designed electrolyte cell the width of the container and the height of the H_2SO_4 electrolyte were the same as the dimensions of the positive plate to ensure a uniform ion flux between positive and negative plates. Since there is excess electrolyte under the experimental conditions, the H_2SO_4 concentration does not change much and neither does the electrolyte specific resistance. It is assumed that the electrolyte specific resistance up and down the plate is uniform during each scan of the reference electrodes from the bottom to top of the positive plate. The data points were acquired every 0.5 cm in height in one scan. Two scans can complete the measurement of one side of the positive plate and 162 data points are obtained. Four scans yield 324 data points on both sides of the positive plate. Therefore, the sum of 324 IR voltage drops obtained in four scans is proportional to the total discharge current of the positive plate and each IR voltage drop measured is proportional to the local current flowing through the electrolyte. When the positive plate is discharged at 45 A, the local current density, i, on the plate can be expressed by

$$i = \frac{45 \times \Delta U}{1.147 \times \sum \Delta U} \tag{1}$$

where ΔU denotes the IR voltage drop measured in the electrolyte, 1.147 cm^2 the measurement area of each point.

When the positive plate is discharged, the difference between the two sides is, in practice, very small. But, the resolution of the reference electrodes and this measurement system is approximately 0.1 mV while the measured IR drops lie in the range between about 300–500 mV at 3 C discharge rate. Thus, small differences between the pasted and non-pasted sides of the positive plate can be distinguished. At the 3 C discharge rate the distributions of current density and potential are quite

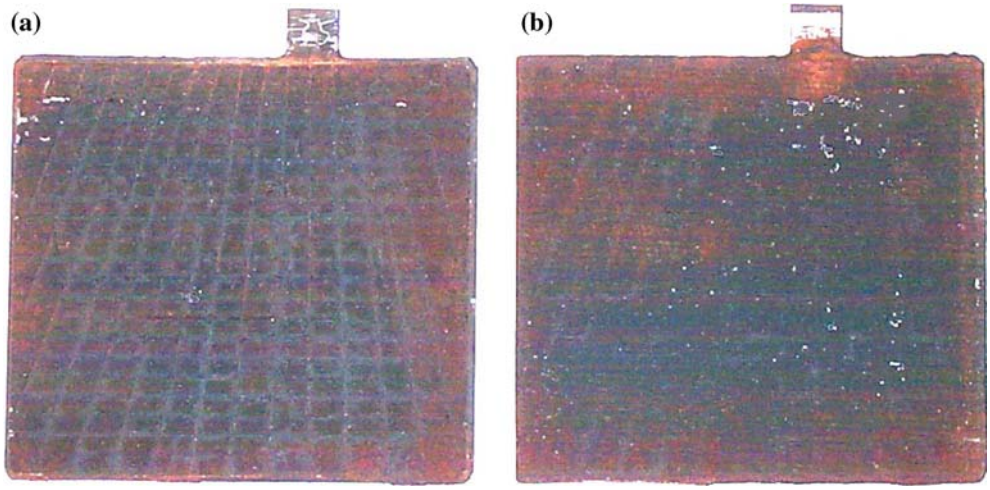

Fig. 1. Photographs of the automotive positive plate with the radiation grid design. (a) non-pasted side; (b) pasted side.

uniform at the beginning of the discharge [28]. However, they become more and more uneven as discharge proceeds. During the discharge interval from 1 to 5 min the current density difference between the pasted and non-pasted sides increases only from 0.7% to 3%. Figure 2 shows the current density distributions on both sides of the positive plate at the 3 C discharge rate at 6 min. Since this is the end of the discharge, the uneven distributions of current density occur on both sides, especially in the upper part of the plate, which is similar to the previously reported results [28]. The current density on the pasted side in Figure 2(a) is higher than that on the non-pasted side in Figure 2(b). Their maximum current density is 148.5 and 128.1 mA cm^{-2} on the pasted and non-pasted sides, respectively. And their average values are 127.1 and 115.3 mA cm^{-2}. The difference between the current densities becomes increasingly large on both sides of the positive plate during discharge. And the depth of discharge on the non-pasted side is lower than that on the pasted side. Figure 3 shows the potential distributions on both sides at the end of discharge. The highest polarization also appears in the upper part of the plate. At the same height of the plate, the distributions of the current density and the potential are almost the same. This is shown in Figures 2 and 3. It appears that the distributions of the current density and the potential on the pasted side are slightly more uneven than those on the non-pasted side. This may be related to the resistance of the extra pasted layer over the grid.

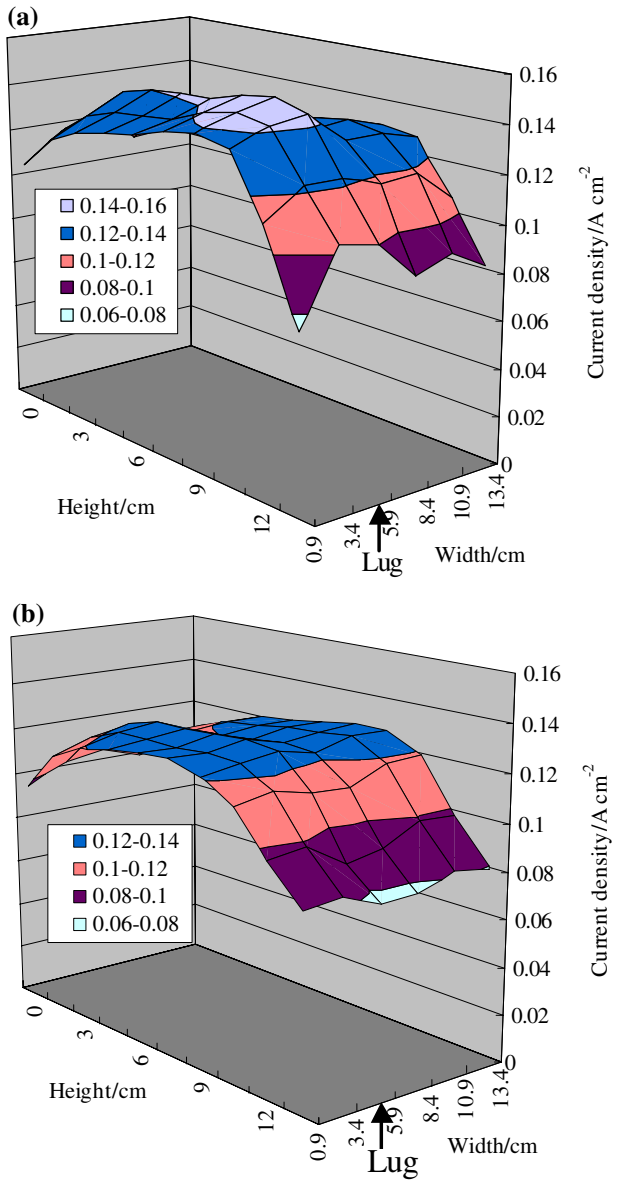

Fig. 2. The current density distributions on the positive plate at 3 C discharge rate. Discharge times: 6 min. (a) pasted side; (b) non-pasted side.

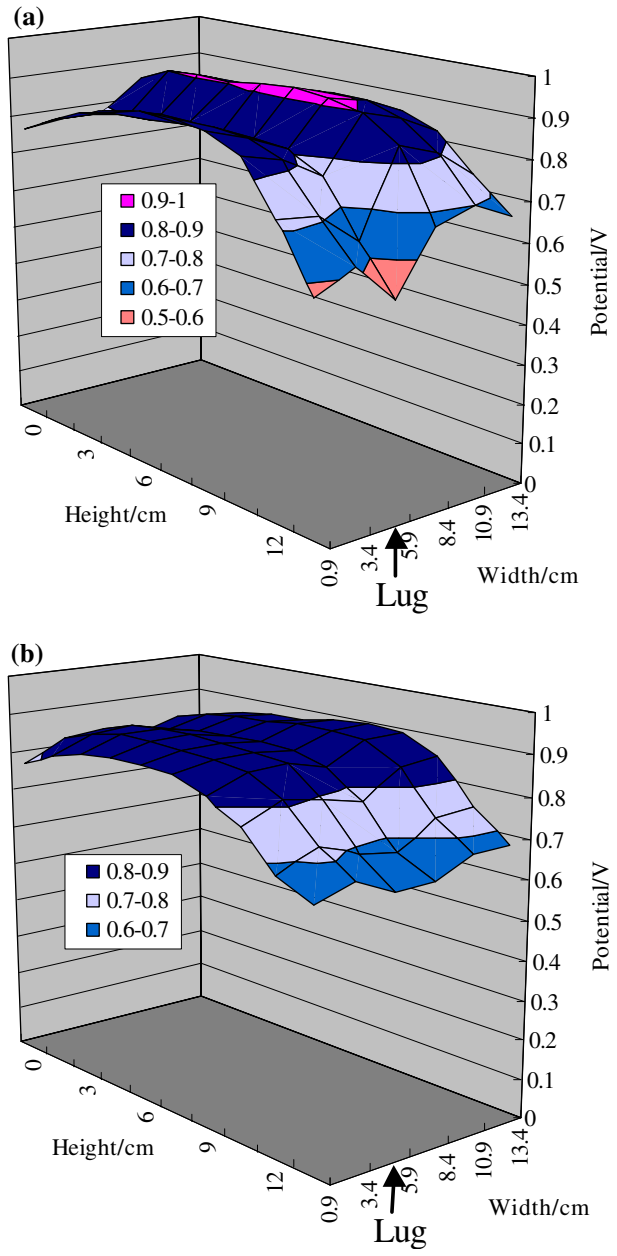

Fig. 3. The potential distributions on the positive plate at 3 C discharge rate. Discharge times: 6 min. (a) pasted side; (b) non-pasted side.

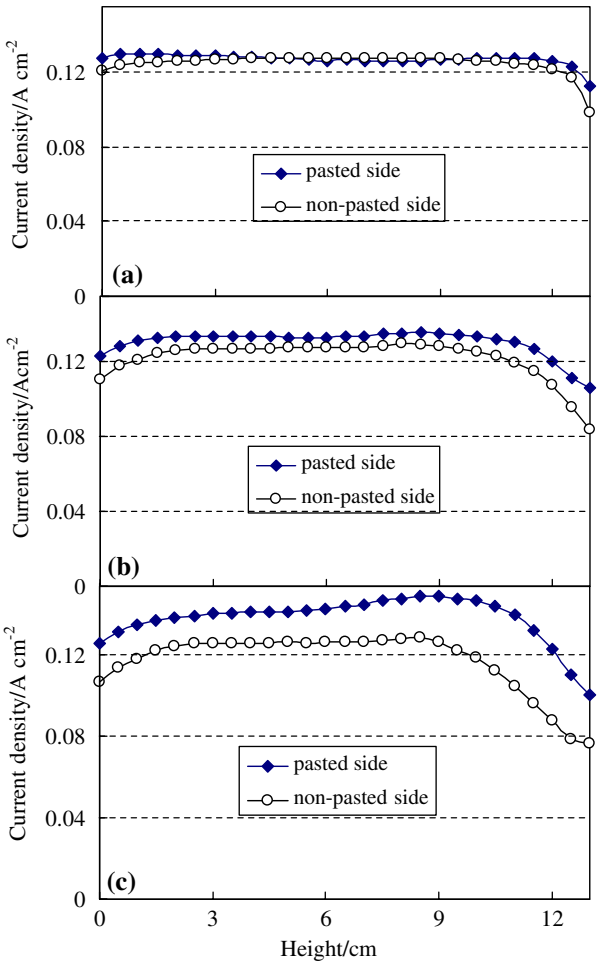

Fig. 4. The evolution of the current density vs. the height in the middle of the two sides of the positive plate at 3 C discharge rate. Discharge times: (a) 1; (b) 5; (c) 6 min.

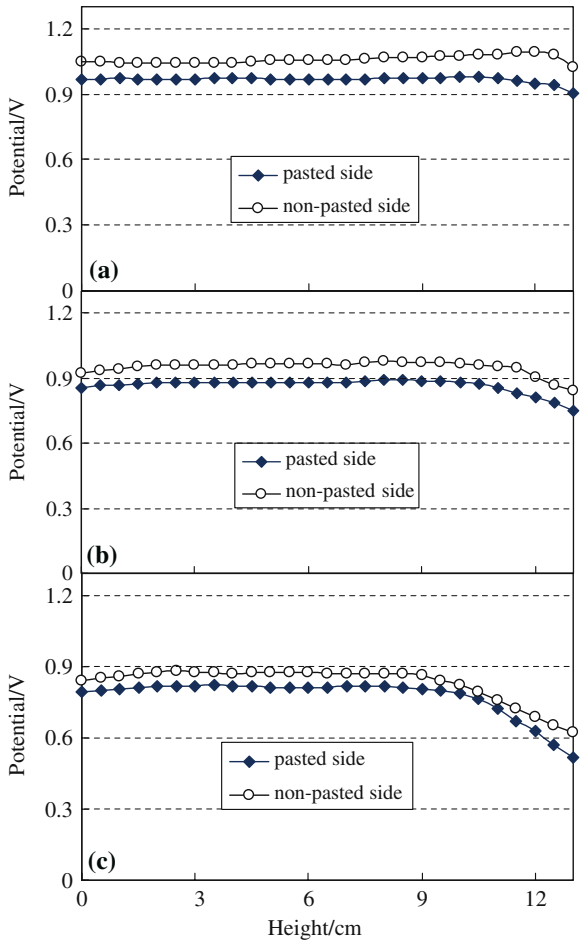

Fig. 5. The evolution of the potential vs. the height in the middle of the two sides of the positive plate at 3 C discharge rate. Discharge times: (a) 1; (b) 5; (c) 6 min.

To compare the difference between the pasted and non-pasted side Figures 4 and 5 show the distributions of current density and potential in the middle of both sides of the positive plate at different times. It is clear from Figure 4(a) that there is hardly any difference between the two sides at 1 min discharge time. But the difference becomes increasingly large as the discharge proceeds as shown in Figure 4(b) and 4(c). On the non-pasted side the current density is almost unchanged in the middle of the plate, but it drops in the lower and upper parts of the plate, especially at the top. Figures 4(b) and 4(c) show that the current density increases on the pasted side as the positive plate is discharged at 45 A. This is attributed to the discharge current being invariant. At the end of the discharge in Figure 4(c), the average current density on the pasted side is 21 mA cm^{-2} higher than that on the non-pasted side. This is to be expected as the pasted side has more active mass and hence higher capacity. This also indicates that the non-pasted side undergoes a deeper depth of discharge than the pasted side during battery cycling. It is well known that the battery life strongly depends on the depth of discharge (DOD). The deeper the DOD the shorter the battery life becomes. Therefore, the active mass under deep discharge on the non-pasted side can accelerate the end of the battery life.

Figure 5 shows that the potential on the non-pasted side is always higher than that on the pasted side. It is evident that the extra pasted layer over the grid has a greater resistance, which leads to a larger IR voltage drop. Thus the higher polarization appears on the pasted side. As the positive plate is discharged at the 3 C rate its potential drops rapidly, especially at the top of the plate and at the end of discharge. And the rates of change of the electrode potentials on the two sides are different. The average potentials are 1.058 and 0.966 V on the non-pasted and pasted sides at 1 min in Figure 5(a), respectively, yet they are 0.830 and 0.774 V at the end of the discharge in Figure 5(c). The average potential difference on the two sides reduces from 92 to 56 mV. This means that the rate of change of the potential on the non-pasted side is faster during discharging, though Figure 4(c) shows that its current density is lower compared with that on the pasted side. It also appears that the non-pasted side has lower capacity and greater electrochemical polarization during the charge-discharge and hence the technology of the single-side pasting is disadvantageous to battery life.

The equilibrium potential on the fully charged positive plate is 1.156 V in the H_2SO_4 electrolyte of 1.285 sp. gr. To obtain the change of the resistance the local polarization specific resistance is defined as the ratio of the polarization to current density. So it can be calculated according to the measured potential and the current density on the positive plate. Figure 6 shows the distributions of the polarization specific resistance in the middle of both sides of the positive plate at different times. As the positive plate is discharged at 3 C rate the polarization specific resistance increases quickly, especially in the upper part of the plate. It is seen from Figure 6(a) that the pasted side has higher polarization specific resistance than the non-pasted side. Their difference reaches about 0.7 Ohm cm^2. This is due to the resistance of the extra paste layer on the pasted side. But the resistance on the non-pasted side increases more quickly than that on the pasted side during discharging. At the end of the discharge in Figure 6(c), the average polarization specific resistance on the non-pasted side is conversely about 0.1 Ohm cm^2 higher than that on the pasted side. This is because there is more active mass on the pasted side and a deeper discharge occurs on the non-pasted side.

On the basis of the current density measured at each location, the current on each side of the plate can be

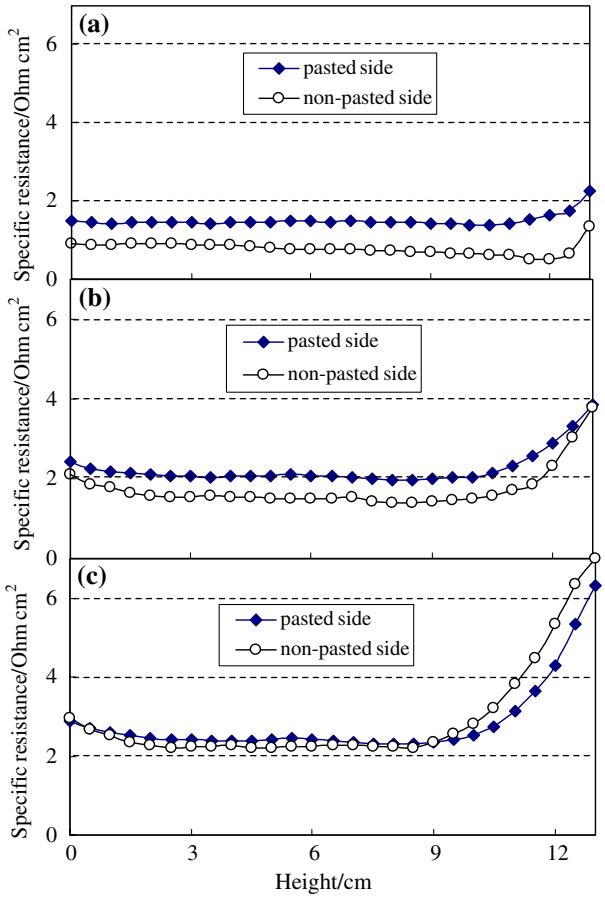

Fig. 6. The evolution of the polarization specific resistance vs. the height in the middle of the two sides of the positive plate at 3 C discharge rate. Discharge times: (a) 1; (b) 5; (c) 6 min.

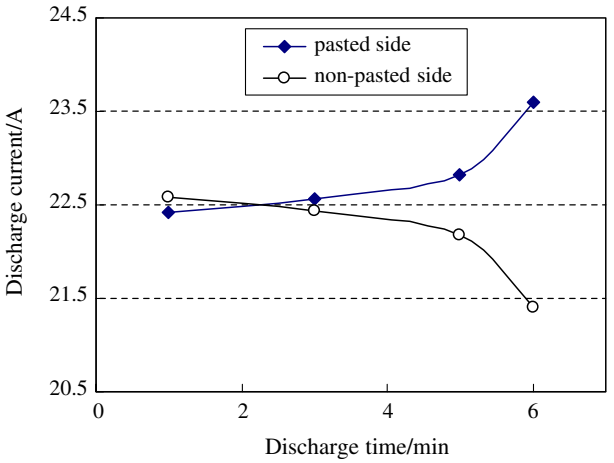

Fig. 7. The evolution of the discharge current on each side of the positive plate at 3 C discharge rate.

calculated when the positive plate is discharged at the 3 C rate. Figure 7 shows the evolution of the discharge current on each side of the positive plate. In the initial stage of the discharge, the pasted side has a high resistance so that a low current appears on the pasted side while a high current occurs on the non-pasted side. On discharging the DOD of the active mass on the non-pasted side increases more quickly, which leads to the falling of the discharge current; whereas the pasted side has more active mass and its DOD is relatively small. So its current contribution increases during discharge because the total discharge current is unchanged. Therefore, for the deep cyclic applications of the batteries, the DOD on the non-pasted side is higher than that on the pasted side, which results in shedding of the active mass on the non-pasted side. The technology of double-side pasting not only reduces the corrosion rate of the positive grid significantly but it is also advantageous to the cyclic life of the battery.

4. Conclusions

The consequence of using single sided pasting machines for plate fabrication is that the front of the grid has more paste than the back. At the initial stage of a 3 C discharge, the current density on the two sides of the positive plate is roughly the same. However, the polarization on the pasted side is higher than that on the non-pasted side because of the resistance of the extra active mass layer over the grid. Since the non-pasted side has no active mass over the grid, the current density drops slowly on the non-pasted side as the discharge proceeds while it increases on the pasted side. This is due to the constant applied discharge current. The extra active mass layer over the grid adds resistance and leads to higher polarization on the pasted side. The extra polarization reaches about 55–90 mV. On the non-pasted side no active mass is pasted over the grid. Without any active material paste over the back of the

grid the corrosion of the positive grid is accelerated. A higher electrochemical polarization also occurs on this side because there is no extra IR drop over the grid. As a result the polarization resistance increases more quickly and the depth of discharge is deeper on the non-pasted side. Therefore, the utilization of the positive active mass on the non-pasted side is also high while its capacity is lower. In this case, its active mass in these regions easily results in the deep discharge and the shedding. So the battery life will be shortened in cyclic applications.

Acknowledgements

The author is grateful to NSFC (No. 20373037) in China for financial support for this work and thanks Dr. Henry Catherino for his assistance with language.

References

1. D. Pavlov and G. Papazov, *J. Electrochem. Soc.* **127** (1980) 2104.
2. S.G. Canagaratna, P. Casson, N.A. Hampson and K. Peters, *J. Electroanal Chem.* **79** (1977) 273.
3. D. Pavlov, I. Balkanov, T. Halachev and P. Rachev, *J. Electrochem. Soc.* **136** (1989) 3189.
4. E.M.L. Valeriote and L.D. Gallop, *J. Electrochem. Soc.* **124** (1977) 370.
5. P. Ekdunge, K.V. Rybalka and D. Simonsson, *Electrochim. Acta* **32** (1987) 659.
6. B.K. Mahato, *J. Electrochem. Soc.* **126** (1979) 365.
7. D. Pavlov and B. Monakhov, *J. Electroanal Chem.* **218** (1987) 135.
8. S. Laihonen, T. Laitinen, G. Sundholm and A. Yli-Pentti, *Electrochim. Acta* **35** (1990) 229.
9. E. Rocca and J. Steinmetz, *J. Electroanal Chem.* **543** (2003) 153.
10. C.S. Lakshmi, J.E. Manders and D.M. Rice, *J. Power Sources* **73** (1998) 23.
11. M. Shiomi, Y. Okada, Y. Tsuboi, S. Osumi and M. Tsubota, *J. Power Sources* **113** (2003) 271.
12. E. Jullian, L. Albert and J.L. Caillerie, *J. Power Sources* **116** (2003) 185.
13. R.D. Prengaman, *J. Power Sources* **95** (2001) 224.
14. P.T. Moseley, *J. Power Sources* **95** (2001) 218.
15. N.E. Bagshaw, *J. Power Sources* **67** (1997) 105.
16. A. D. Turmer, P. T. Moseley and J. L. Hutchison, Proceedings-The Electrochemical Society, v 84–14, (1984) 267.
17. D.C. Constable, J.R. Gardner, K. Harris, R.J. Hill, D.A.J. Rand and J.B. Zalcman, *J. Electroanal. Chem.* **168** (1984) 395.
18. L.T. Lam, N.P. Haigh, D.A.J. Rand and J.E. Manders, *J. Power Sources* **88** (2000) 2.
19. Yu. Kamenev, N. Chunts and E. Ostapenko, *J. Power Sources* **116** (2003) 169.
20. I. Dyson and P. Griffin, *J. Power Sources* **116** (2003) 263.
21. L. Prout, *J. Power Sources* **41** (1993) 107.
22. H. Ozgun, L.T. Lam, D.A.J. Rand and S.K. Bhargava, *J. Power Sources* **52** (1994) 159.
23. A. Rochliadi and R. De Marco, *J. Applied Electrochem.* **32** (2002) 1039.
24. A. Rochliadi, R. De Marco and A. Lowe, *J. Appl. Electrochem.* **34** (2004) 263.
25. K.R. Bullock, B.K. Mahato and W.J. Wruck, *J. Electrochem. Soc.* **138** (1991) 3545.
26. D. Pavlov and N. Kapkov, *J. Electrochem. Soc.* **137** (1990) 17.
27. W.H. Kao, P. Patel and S.L. Haberichter, *J. Electrochem. Soc.* **144** (1997) 1907.
28. Y. Guo, Y. Li, G. Zhang, H. Zhang and J. Garche, *J. Power Sources* **124** (2003) 271.
29. Y. Guo and J. Garche, *J. Electrochem. Soc.* **152** (2005) A622.